http://dx.doi.org/10.5012/bkcs.2013.34.8.2466

Characterization of Binding Mode of the Heterobiaryl gp120 Inhibitor in HIV-1 Entry: A Molecular Docking and Dynamics Simulation Study

Changdev G. Gadhe,[†] Gugan Kothandan,[†] and Seung Joo Cho[†,‡,*]

Departments of [†]Bio-New Drug Development and [‡]Cellular·Molecular Medicine, College of Medicine, Chosun University, Gwangju 501-759, Korea. [*]E-mail: chosj@chosun.ac.kr
Received May 5, 2013, Accepted May 30, 2013

Human immunodeficiency virus type-1 (HIV-1) is a causative agent of Acquired immunodeficiency syndrome (AIDS), which has affected a large population of the world. Viral envelope glycoprotein (gp120) is an intrinsic protein for HIV-1 to enter into human host cells. Molecular docking guided molecular dynamics (MD) simulation was performed to explore the interaction mechanism of heterobiaryl derivative with gp120. MD simulation result of inhibitor-gp120 complex demonstrated stability. Our MD simulation results are consistent with most of the previous mutational and modeling studies. Inhibitor has an interaction with the CD4 binding region. Van der Waals interaction between inhibitor and Val255, Thr257, Asn425, Met426 and Trp427 were important. This preliminary MD model could be useful in exploiting heterobiaryl-gp120 interaction in greater detail, and will likely to shed lights for further utilization in the development of more potent inhibitors.

Key Words : HIV-1, gp120, Heterobiaryl inhibitors, Molecular docking, MD simulation

Introduction

Human immunodeficiency virus type 1 (HIV-1) infect millions of people worldwide and is the cause of the lethal disease, Acquired Immune Deficiency Syndrome (AIDS).[1-3] Gp120 is an intrinsic protein for viral entry to host cell, which has four domains, distal, proximal, inner and outer. The bridging sheet (β2, β3, β20 and β21) is a part of inner domain. Sequences of gp120 of immunodeficiency viruses identified from different species shows five variable loops (V1-V5).[4] The disulfide bridges are at the bases of the V1-V4 loops, which are exposed to outer environment.[5] It is known that the conformation of gp120 V3 loop changes upon cluster for differentiation 4 (CD4) binding, which expose and/or forms the binding sites for chemokine receptors. The chemokine receptors CCR5 and CXCR4 mediate viral entry to host cell.[6]

The viral entry process consists of three steps; first, viral attachment to host CD4 receptor; second, chemokine receptor binding; and third, fusion of virus and host cell, which together presents a number of druggable targets for new drug discovery prior to cellular infection.[7-9] The first step of viral entry usually consists of attachment of CD4 to HIV-1 envelope glycoprotein, which contains a trimer of dimers of two subunits gp41 and gp120.[10] It is well known that CD4 binds to gp120 with high affinity,[11] and the interaction takes place through the N-terminal extracellular domain of CD4.[12] CD4 is a 55-kDa glycoprotein that consists of four extracellular domains called D1-D4, one transmembrane domain, and a cytoplasmic tail. The attachment step is followed by conformational changes, in V3 loop of gp120 that binds to chemokine CXCR4 and CCR5 coreceptors. After conformational changes, gp41 triggers out and fuses the viral and host cell membrane and pours out all the viral material into the host cell cytosol.[13,14] It has been reported that the stabilization of the first two domain of CD4 (CD4D12)-gp120 complex through interchain disulfide exchange lead to an increase in the efficacy of viral entry inhibition.[15]

Numerous crystal structures have been reported for the CD4-gp120 complex.[16-22] It is also well known that this complex consists of a highly conserved interacting cavity. It has been illustrated that for new drug development against HIV-1, CD4-gp120 cavity is a good source.[16,23] Bristol-Myer-Squibb (BMS) pharmaceutical has discovered a small molecule inhibitor (**BMS-378806**) against gp120.[24,25] Numerous research groups used genetic, biochemical and virus infection based approaches on BMS and related inhibitors to identify their binding location on gp120.[9,26,27] Also, number of molecular modeling techniques such as quantitative structure activity relationship (QSAR), docking, and molecular dynamics were used to understand the mechanism of action of inhibitors in the gp120 cavity.[28-31] Our group is also actively involved into the modeling study of important pharmaceutical drug targets. we performed homology modeling, QSAR, docking and MD simulation techniques to study important drug targets.[32-40]

Previously reported **BMS-378806** is a prototype of compound of heterobiaryl gp120 inhibitors.[41] **BMS-378806** and its analogues are of high interest because of their higher potency and smaller size. Currently used heterobiaryl inhibitors are differed from the **BMS-378806** by replacement of azaindole group with the heterobiaryl group. However, it was observed that the certain variations in **BMS-378806** substitution pattern of the azaindole and indole ring are tolerated.

In addition to the above mentioned reports, this manuscript contains docking and MD simulation studies of heterobiaryl inhibitor and gp120 as HIV-1 entry inhibitor. Docking studies for the most potent inhibitor was done, and

further 50000 ps MD simulation was performed in an explicitly solvated box. MD simulation was performed for the ligand-gp120 to determine the stable binding mode of heterobiaryl inhibitor into the gp120, and also to provide insight into the interaction mechanism of these inhibitors. Long simulation time was chosen for sufficient sampling of occurrence of ligand-gp120 interactions.

Materials and Methods

Preparation of Small Molecular Inhibitor and Protein Structure. The most potent inhibitor (**13h**) (Figure 1), of the dataset[41] was drawn using SYBYL 8.1[42] software package. Minimization was performed with the Tripos force field using 1000 steps of steepest descent algorithm followed by the 1000 steps of conjugate gradient algorithm. The partial atomic charges were applied using Gasteiger-Hückel method. Systematic search on all the rotatable bonds were carried out using 30 rotations. From the ensemble of conformations, a lowest energy conformation was selected for the further docking process. In order to locate the putative binding site of **13h** into gp120, docking experiment to the crystal structure of gp120 (4DKR, 1.8 Å) was performed.[22] First, 4DKR was extracted from the brookhaven protein data bank (PDB) and then the co-crystallized ligand was removed using biopolymer module of SYBYL. Then the amide bonds of GLN and ASN were flipped using SYBYL and the resultant structure of gp120 was saved as a PDB coordinates. Flipping of ASN/GLN is useful when dealing with the poorly resolved X-ray crystal structures, in which there are higher chances of incorrect determination of the oxygen and nitrogen atoms. This type of mis-fitting changes both hydrogen-bonding and steric consideration (NH2 occupies more space than the O).[43] Therefore, we flipped ASN/GLN by 180° using SYBYL biopolymer module.

The gp120 structure was then relaxed by minimizing 1000 steps of steepest descent algorithm followed by 1000 steps of conjugate gradient algorithm with the aim to remove strain from the X-ray structure and subsequently used for further docking and dynamics simulations study.

Molecular Docking of Inhibitor into the gp120. To evaluate the binding modes of heterobiaryl inhibitor into gp120, molecular docking studies were performed using Autodock 4 software package.[44] The non-polar hydrogen atoms of gp120 were merged and only polar hydrogen atoms were kept for docking study using Autodock Tools (ADT). The putative binding pocket for the inhibitor docking in gp120 was defined according to the previously published mutagenesis reports,[9,26,45,46] This site is similar to the cocrystalled ligand binding site on gp120. According to the data from previous mutational studies, Trp427 is an important residue, which is situated in the gp120 cavity, and therefore a center of grid was assigned to C_α atom of Trp427. The grid spacing of 0.0375 nm was used with the 50 × 50 × 50 grid points in each dimension. Autodock default parameters were used and 100 independent docking runs were carried out for the **13h**. All the rotatable bonds of **13h** were set free to rotate inside gp120 during docking simulation. At the end of docking simulation, cluster analysis was performed on all the docked poses. All docking solutions of ligand all-atom root mean square deviation (RMSD) with 0.2 nm of each other were clustered and ranked by the lowest energy. The representative binding mode from docking calculations was selected as a lowest energy cluster.

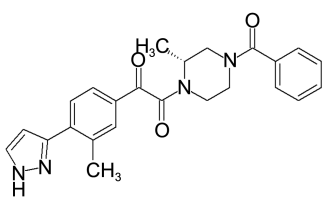

Figure 1. Chemical structure of **13h**.

General MD Simulation Setup. All the MD simulations were performed using GROMACS 4.5.3 package[47] and 53a6 GROMOS force field.[48] Topology and coordinates of ligand (**13h)** was generated using the PRODRG (http://davapc1.bioch.dundee.ac.uk/prodrg/) server.[49] Water molecules were represented by SPC water model.[50] The complex structure was solvated in a cubic box with the consideration of minimum distance between protein and box wall of 1.0 nm. Cubic box containing complex structure was solvated with 21516 water molecules. Using program genion, two chloride atoms were added at points with most favorable electrostatic potential to neutralize the system, resulted in 67648 atoms in the system. The system was energy minimized to remove excessive strain. First, we performed 5000 steps of steepest descent minimization with restraints (with a force constant of 1000 kJ mol^{-1} nm^{-1}) applied to all atoms. The time step for integrating the equations of motion was 0.002 ps. A cutoff of 1.4 nm was used for van der Waals interactions and a smooth particle mesh Ewald method[51] was used for long-range electrostatic interactions beyond a 0.9 nm cutoff. The neighbor lists were updated every 10 steps. The SETTLE algorithm[52] was used to keep water molecules rigid and the LINCS algorithm[53] was employed to keep all remaining bonds at their equilibrium lengths. The Berendsen coupling algorithm was used to keep constant temperature and pressure conditions throughout the simulations.[54] The pressure coupling constant used was 0.5 ps and the compressibility was set to 4.5×10^{-5} bar^{-1} while the heat coupling constant was set to 0.1 ps. There was a separate coupling of solutes and solvent baths. The simulation system was first stabilized for temperature and pressure. A 100 picoseconds (ps) NVT (constant volume and temperature) simulation was performed followed by 100 ps NPT (constant pressure and temperature) simulation. It is necessary to maintain temperature of the system for certain period and then pressure should be calculated. The reason is that the calculation of pressure at low temperature could be inaccurate. Hence, first NVT simulation was performed to stabilize temperature, and later on NPT simulation for 100 ps was performed with 300 K temperature and 1 bar pressure. Also, we checked void spaces after NVT and NPT simulations and found that there were no void spaces. Then, final production run of 50000 ps

were invoked for ligand-gp120 complexes by maintaining temperature and pressure.

Results

Molecular Docking Analysis of the Heterobiaryl Inhibitor into gp120. To elucidate the detailed interaction mechanism between heterobiaryl inhibitor and gp120, molecular docking studies were performed using Autodock. A putative binding pocket was defined based on previously published mutagenesis reports.[9,26,45,46] According to these reports, the binding pocket for CD4 as well as small molecular antagonists consist of the Trp112, Thr257, Asp368, Glu370, Ile371, Ser375, Asn425, Met426 and Trp427 residues (Figure 2). The given Autodock protocol was used to generate one hundred docking solutions for **13h** into the gp120. The pose was selected based on the lowest energy cluster. One representative binding mode of **13h** was selected from the more negative binding energy cluster. Selected binding mode of the **13h** is shown in Figures 3. Surrounding 4 Å residues were shown for the clarity. Overlapped binding mode of the **13h** (IC_{50} = 35 nM) and 4DKR cocrystalled ligand are shown in Supp Info S1. **13h** docked into the pocket formed by the residues Trp112, Val255, Thr257, Glu370, Ile371, Ser375, Phe376, Asn377, Phe382, Phe383, Tyr384, Ile424, Asn425, Met426, Trp427, Thr430, Gly473 and Ile475. **13h** predominantly interacts through the hydrophobic interactions. **13h** identified similar residues as cocrystalled ligand. Careful scrutiny of binding pose shows that the pyrazole ring of **13h** is docked deep inside the pocket. 3-methyl-phenyl of **13h** was docked into a hydrophobic pocket which was lined by the residues Thr257, Glu370, Phe382, Tyr384, Asn425, Met426 and Trp427. Pyrazole ring of the **13h** was found to be docked deep inside the crevice formed by the residues Val255, Thr257, Asn377, Phe382. The benzoyl ring of **13h** interacted with Val430, whereas the piperazine interacted with the main chains of Trp427 and Glu429.

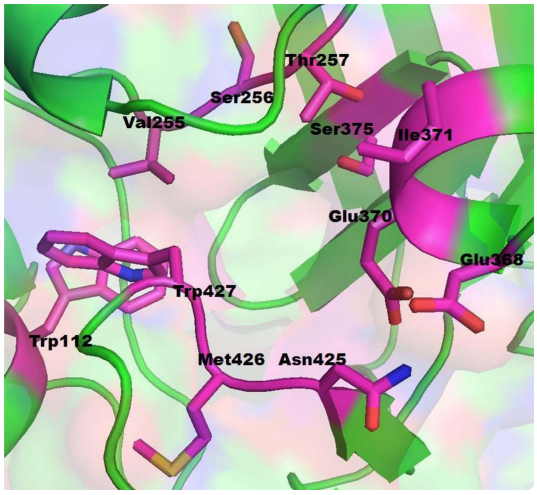

Figure 2. Constructed binding pocket of gp120 for docking experiment of **13h**.

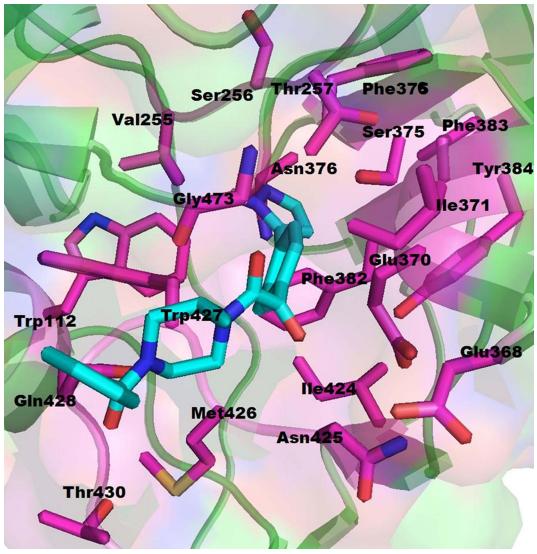

Figure 3. Docked mode of the **13h** into gp120 active site. gp120 is shown in transparent green cartoon, active site residues in 4 Å are shown by magenta stick and **13h** shown in cyan. Figure generated using Pymol program (www.pymol.org).

MD Simulation Analysis. MD simulation for the selected inhibitor (**13h**) was done for long duration (50000 ps) using Gromacs software package. Before starting the long duration simulations, it was confirmed that the systems were stabilized for temperature (300 K) and pressure (1 bar) (Supp Info S2). The gp120 backbone atoms RMSD in simulated system was monitored as a function of time and depicted in Figure 4(a). Protein structure stability during MD simulation was monitored by calculating the potential energy, which is shown in Figure 4(b). Figure 4(a) represents the backbone atoms RMSD for gp120 in simulated system. It was observed that in **13h**-gp120 system, the protein structure was equilibrated for first 5000 ps and RMSD was found to be continuously rising upto 0.225 nm. After equilibration, the RMSD was gradually decreased upto 20000 ps and again increased and leveled off for the rest of simulation period. The RMSD of the backbone of gp120 was found to be ~0.205 nm.

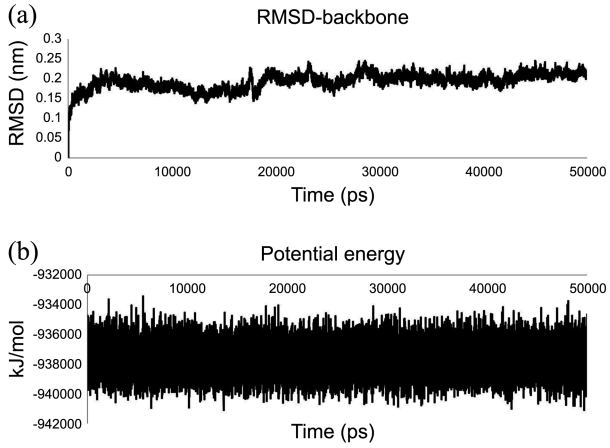

Figure 4. RMSD and potential energy. (a) Backbone RMSD of **13h** as a function of time. (b) Potential energy of the gp120 in simulated system as a function of time.

The stability of the gp120 structures during MD simulations was monitored through potential energy plot (Figure 4(b)) as a function of time. Gromacs utility g_energy was used to calculate the potential energy, total energy and temperature. Figure 4(b) represents the potential energy graphs for the gp120 in simulated system. For the **13h**-gp120, potential energy fluctuated between −933428 to −941076 kJ/mol, with an average potential energy of −937578 kJ/mol. From the potential energy graphs it is evident that all the structures are stable and found to be configured in very small energy difference. Pressure and total energy of system were monitored during MD simulation and graphically plotted in Supp Info S3. For the simulated system (**13h**-gp120), total energy was observed in the range from −764306 kJ/mol to −773445 kJ/mol, with an average of −768914 kJ/mol. From the energy analysis it is evident that the all structures were stable throughout the simulation with very little deviation in energy. Pressure plot denotes that throughout the simulation period average pressure of system was 1 bar.

Root Mean Square Fluctuations (RMSF) Analysis. Temperature of the system (**13h**-gp120) during 50000 ps simulation was monitored to confirm that the simulation was performed at a constant temperature of 300 K. Time dependent temperature plot of the simulated system was shown in Figure 5(a). RMSF of gp120 residues were monitored throughout simulations and plotted in Figure 5(b). MD simulations trajectories were used to elucidate the fluctuation profiles of all the residues in simulated system (**13h**-gp120) by using Gromacs utility g_rmsf. From the Figure 5(b), it is evident that the residues near to the missing loop regions have been fluctuated with the more intensity. It has been observed that the α helical regions and β sheets were most stable during long duration simulations, which may be because of intermolecular hydrogen bonding and disulfide bridges. Most of the residues were fluctuated with the intensity less than 0.3 nm. Very few residues were fluctuated with the intensity more than 0.3 nm, which belong to the N-terminal region, C-terminal region, near residues of V1/V2 loop and other loop regions.

RMSDs of the Inhibitors and Radius of Gyration (Rg). All atom RMSDs of the inhibitor was calculated as a function of time and reported in Figure 6(a). RMSD for the simulated inhibitor was calculated by the mean of g_rms utility of Gromacs. It was observed that the **13h** is stable throughout the simulation period with an average RMSD of 0.075 nm. However, it was also noted that the RMSD fluctuated between 0.02 nm to 0.18 nm, which indicates that ligand binds tightly in gp120 cavity. Protein structure stability is measured as a compactness of protein throughout simulation period. Gromacs utility g_gyrate was used to calculate the compactness of protein structure (Rg). Rg of the gp120 in simulated system was calculated and reported in Figure 6(b). For **13h**-gp120 system, Rg of gp120 was decreased upto ~13000 ps, and again rose upto 38000 ps and again slowly decreased afterwards. It indicates that the compactness of gp120 was increased initially and later on slowly diminished, and finally increased after ~38000 ps.

Binding Mode Analysis of the Inhibitor after MD Simulation. Average binding mode of the **13h**-gp120 was generated after MD simulation using last 10000 ps trajectory. The obtained structure tends to be crude hence energy minimization was performed to remove bad contacts. 4 Å residues in vicinity of simulated inhibitor were shown for clarity. The MD simulated binding mode for **13h**-gp120 has been shown into the Figure 7. The base of the binding pocket is constructed with hydrophobic residues such as Phe382, Met426, Trp427 and Tyr435, whereas the deep inside pocket sidewall was lined by the Val255, Thr257, Glu370, Ile371, Gly473, Asn474 and Ile475. The opening gate of the pocket was lined by Glu370, Asn425, Met426, Trp427, Gly473 and Ile475 residues. However, the benzoyl part of the **13h** was stabilized by outside of the binding pocket lined by the residues Met426, Trp427, Gln428, Glu429 and Val430. 3-methyl phenyl of **13h** was stabilized into a hydrophobic pocket of Trp427, Phe382 and Tyr435. However, Lenard-Jones and Columbic interactions between **13h** and surround-

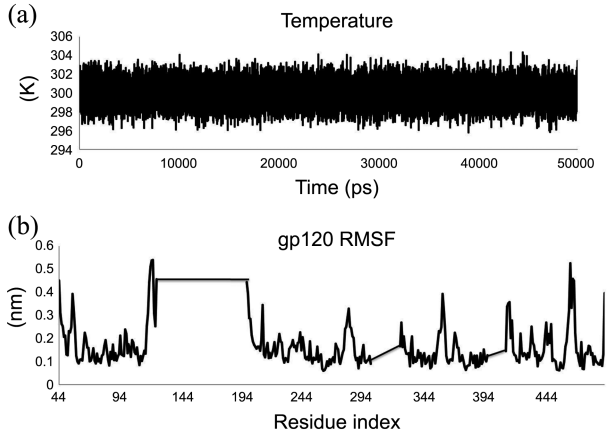

Figure 5. Temperature and RMSF of the simulated systems. (a) Temperature of the simulated systems as a function of time. Average temperature of system was 300 K. (b) RMSF of the gp120 in simulated system.

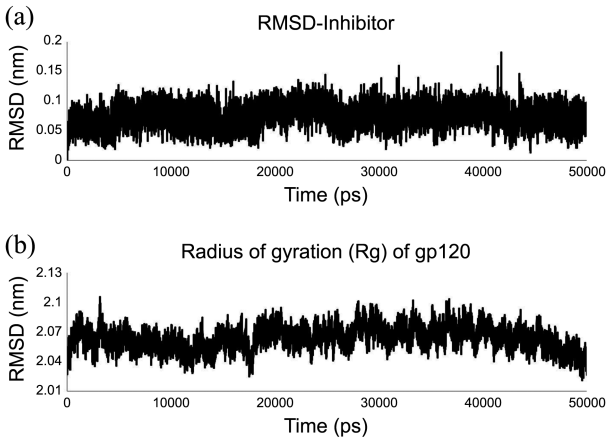

Figure 6. Inhibitors RMSD and radius of gyration (Rg). (a) All atoms RMSD of **13h** as a function of time. (b) Radius of gyration of gp120 in simulated system plotted as a function of time.

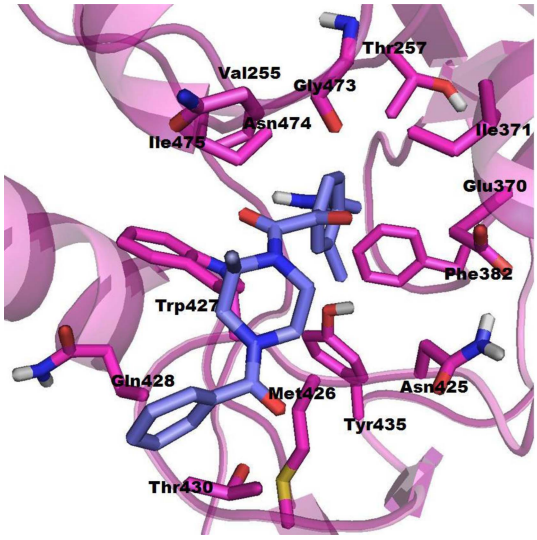

Figure 7. MD simulated average binding mode of the **13h** into gp120. Active site residues in the vicinity of 4 Å of **13h** were shown in magenta stick, whereas, **13h** is shown in violet stick. gp120 is shown in transparent magenta cartoon.

Table 1. Short range Lennard-Jones (LJ) and Columbic interactions between **13h** and surrounding residues of gp120

Residue Index	LJ-SR (kJ/mol)	Coul-SR (kJ/mol)
Val255	-11.54	1.023
Thr257	-9.884	-0.099
Glu370	-12.60	-1.083
Ile371	-4.469	-0.030
Phe382	-4.577	-2.706
Asn425	-7.448	-14.99
Met426	-10.17	-0.872
Trp427	-30.14	-3.225
Gln428	-5.830	-0.122
Thr430	-7.817	-0.069
Tyr435	-0.308	0.006
Gly473	-9.575	1.833
Asn474	-9.328	0.002
Ile475	-12.34	-7.117

ing 4 Å gp120 residues were calculated and shown in Table 1.

Minimum Distances between Inhibitor and Binding Site Residues. Simulated inhibitor interacted through the hydrophobic interactions. So, we calculated the minimum distances between ligands and interacting residues. Gromacs utility g_mindist was used to get the distance between two groups. In MD simulation, it was observed that some of the identified residues during docking study were vanished.

The minimum distances between **13h** and gp120 active site residues were calculated as a function of time and plotted in Figure 8. For most of the residues, the average minimum distances between **13h** and the surrounding residues of the active site are less than 0.4 nm. However, for a few of the active site residues the minimum average distance from **13h** exceeded 0.4 nm. Residues such as Val255, Thr257, Glu370, Phe382, Asn425, Met427, Thr430, Gly473 and Ile475 were

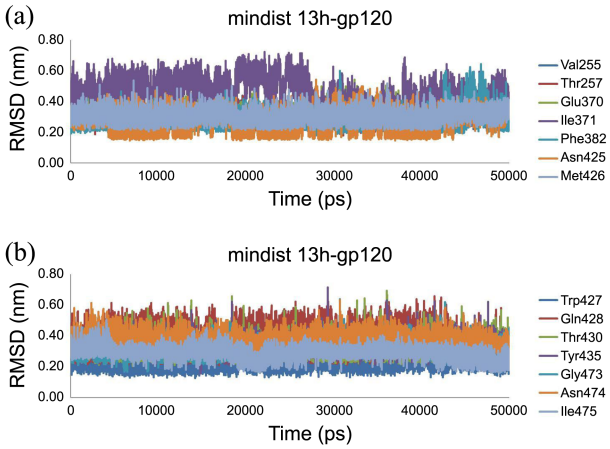

Figure 8. Calculated minimum distances between **13h** and the surrounding residues were plotted as a function of time.

found to have a minimum distance of less than the 0.4 nm throughout the simulation time. However, residues Ile371, Phe382, Gln428 and Asn474 showed more than 0.4 nm average minimum distances from **13h**. From this analysis it is evident that the most of the active site residues were closer than the 0.4 nm throughout the simulation. It is obvious that Gln428 and Met426 have variable minimum distances with the **13h** because they have side chains facing outside the pocket.

Discussion

In this study we performed docking of heterobiaryl inhibitor into gp120 using Autodock. Docking study was performed with the assumption of rigid receptor and flexible ligand. The limitation of rigid docking is, if the inhibitor changes gp120 structure, such changes cannot be visible in docking calculations. Therefore, identified pose is largely based on the rigid interactions. To overcome this situation, a MD simulation was performed in which both ligand and gp120 are set completely free to interact and there by mimicking the natural environment of drug-protein interaction *in vivo*. The most potent inhibitor (**13h**) of the dataset was selected for the binding mode analysis and simulated for 50000 ps. MD simulation results were analyzed, which showed that the **13h**-gp120 complex was fairly stable throughout simulation period. Inhibitor RMSD was calculated, which indicated that simulated inhibitor was stable with overall lower RMSD. It was also observed that the **13h**-gp120 interactions are mainly hydrophobic in nature. Table 1 show that the calculated Lennard-Jones and Columbic interaction between inhibitor and active site residues. It was observed that Trp427 (–30.14 kJ/mol) shows maximum steric interactions among the other residues. Previously it has been reported that Trp427 is an important residue, and it interacts through the stereo-electronic interactions.[16,30] Trp427 shows –3.225 kJ/mol electrostatic interaction energy, which indicates it has less electrostatic interactions than steric. Higher steric interactions were noted for the Glu370 (–12.60 kJ/mol), Ile475

(−12.34 kJ/mol), Val255 (−11.54 kJ/mol) and Met426 (−10.17 kJ/mol). It was observed that side chains of Glu370 sterically interacted with the benzoyl of inhibitor. Calculated electrostatic interaction energy for Glu370 (−1.083) indicates that it has less contribution in ligand-receptor interaction. Higher electrostatic interaction energy was calculated for Ile475 (−7.117 kJ/mol), which indicates that there might be hydrogen bond formation occurs between main chain of Ile475 and carbonyl of ligand during MD simulation. Val255 has higher steric interactions (−11.54 kJ/mol) which is in line with previous report indicating that Val255 is an important residue in the deep pocket for CD4 binding as well as gp120 inhibitors binding.[16,30,55] The side chain of Met426 is facing outside of the binding cavity and it interacts through the main chain atoms with inhibitor (−10.17 kJ/mol). Higher electrostatic interaction was observed for Asn425 (−14.99 kJ/mol). Side chain of Asn425 is facing towards the gate of binding pocket and may interact electrostatically with pyrazole of inhibitor.

Previous reports stated that Phe43 is an important residue in the interaction between gp120 and CD4 for viral entry into the host cells.[56,57] Simulated binding mode signifies that **13h** penetrated deep into the gp120 crevices with the similar insertion of angle compared to cocrystalled ligand of 4DKR. It also pointed that the use of long duration MD simulation to identify stable binding mode similar to 4DKR cocrystalled ligand (Figure 4(a), 6(a)). In addition, **13h** (IC_{50} = 35 nM) shows stable binding mode, which targets the CD4 binding site, but do not show interactions with another hotspot on gp120 (Asp368). However, previous studies also verified that mutation of the binding site residues of **BMS-378806** and CD4 of gp120 abolish the binding of **BMS-378806** and soluble 4-domain CD4 (sCD4).[16] Other previous studies have shown that **BMS-378806** binds in a CD4-binding pocket of the viral gp120 and inhibit viral attachment.[9,22,27,30] Thus, we could assume a similar mode of action for **13h**, because **13h** have similar scaffold like **BMS-378806** and the only difference is that the indole ring is substituted by heterobiaryl. Our results are consistent with the above-mentioned reports, indicating that inhibitor binds in CD4-binding region on gp120. However, previous report by Stricher *et al*.,[58] is in contrast with our results, which show that the **BMS-378806** does not target Phe43 binding site or CD4 binding area on the gp120.

RMSF (Figure 5(b)) for gp120 in simulated systems was calculated, which indicated that the near residues of missing V1/V2 and V3 loop has more movement. The bridging sheet (β2, β3, β20 and β21) of gp120 in simulated system was found to be stable. It was also observed that **13h** forms close contact (Figure 7) with the bridging sheet residues (Asn425, Met426, Trp427 and Thr430). However, current MD simulation study shows that in the presence of ligand in CD4 binding region, such movement of β20/β21 sheet and α-1 helix is forbidden. This observation is consistent with the recently reported gp120 structure in presence of cocrystalled ligand.[22] Calculated Lennard-Jones and Columbic interactions indicates that the ligand-protein interactions are more steric (Trp427, Glu370, Ile475, Val255, Met426, Gly473, Asn474 and Thr257) and less electrostatic (Asn425, Ile475 and Trp427) in nature. Closer van der Walls interactions were observed with the α-1, α-5, β20/β21 sheet, inner domain and outer domain residues.

In summary, heterobiaryl inhibitor appears to be a new class of HIV-1 inhibitors, which could obstruct the CD4-gp120 interaction by specifically targeting the CD4 binding domain on gp120. Current MD simulation result is in agreement with most of the previous mutational and modeling reports. In this study, docking directed MD simulation method was used to identify stable binding mode of the heterobiaryl inhibitor in gp120 cavity.

Conclusion

In this study, binding mode of the heterobiaryl inhibitor (**13h**) into the gp120 active site was analyzed. Binding mode of the inhibitor was selected from the lowest energy cluster. Further simulation of the ligand-gp120 complex was performed for long duration (50000 ps) to know the interaction mechanism. Average binding mode of the simulated inhibitor was scrutinized, and found a stable binding mode in the simulated system. Our results are in line with most of the previous reports. It was observed that the heterobiaryl inhibitor interacted through the stereo electronic interaction with the gp120 binding site. Calculated Lennard-Jones and Columbic interactions for ligands and active site residues revealed that the van der Waals interactions are crucial for this series of compound. However, Val255, Thr257, Glu370, Asn425, Met426 and Trp427 were found to interact maximally with the inhibitor. RMSF of gp120 shows that the near residues of V1/V2 and V3 loop show more fluctuations as compared to α helices and β sheet region. Backbone RMSDs of gp120 and all atom RMSDs of inhibitor are less than ~0.3 nm, indicating stability of ligand-gp120 complex throughout the simulation.

Our results present an integrated atomic overview of heterobiaryl inhibitors and it may be useful in understanding the in depth mechanism of interactions of this inhibitor with gp120, and assist in rational drug design against viral entry. This preliminary MD model could be useful in exploiting heterobiaryl-gp120 interaction in greater detail, and in shedding lights on interactions that can be further utilized in the development of more potent inhibitors. From this study, it appears that combining docking and MD simulation provides more accurate and informative way to assess ligand-gp120 interaction.

Acknowledgments. This study was supported by the research fund from Chosun University 2013.

References

1. De Clercq, E. *J. Med. Chem.* **1995**, *38*, 2491.
2. Gallo, R. C.; Salahuddin, S. Z.; Popovic, M.; Shearer, G. M.; Kaplan, M.; Haynes, B. F.; Palker, T. J.; Redfield, R.; Oleske, J.; Safai, B. *Science* **1984**, *224*, 500.

3. Barré-Sinoussi, F.; Chermann, J. C.; Rey, F.; Nugeyre, M. T.; Chamaret, S.; Gruest, J.; Dauguet, C.; Axler-Blin, C.; Vézinet-Brun, F.; Rouzioux, C. *Science* **1983**, *220*, 868.
4. Starcich, B. R.; Hahn, B. H.; Shaw, G. M.; McNeely, P. D.; Modrow, S.; Wolf, H.; Parks, E. S.; Parks, W. P.; Josephs, S. F.; Gallo, R. C. *Cell* **1986**, *45*, 637.
5. Leonard, C. K.; Spellman, M. W.; Riddle, L.; Harris, R. J.; Thomas, J. N.; Gregory, T. *J. Biol. Chem.* **1990**, *265*, 10373.
6. Moore, J. P. *Science* **1997**, *276*, 51.
7. Moore, J. P.; Doms, R. W. *Proc. Natl. Acad. Sci. U.S.A.* **2003**, *100*, 10598.
8. Blair, W. S.; Lin, P. F.; Meanwell, N. A.; Wallace, O. B. *Drug Discov. Today* **2000**, *5*, 183.
9. Guo, Q.; Ho, H. T.; Dicker, I.; Fan, L.; Zhou, N.; Friborg, J.; Wang, T.; McAuliffe, B. V.; Wang, H. H.; Rose, R. E. *J. Virol.* **2003**, *77*, 10528.
10. Dalgleish, A. G.; Beverley, P. C. L.; Clapham, P. R.; Crawford, D. H.; Greaves, M. F.; Weiss, R. A. *Nature* **1984**, *312*, 763.
11. Lasky, L. A.; Nakamura, G.; Smith, D. H.; Fennie, C.; Shimasaki, C.; Patzer, E.; Berman, P.; Gregory, T.; Capon, D. J. *Cell* **1987**, *50*, 975.
12. Berger, E. A.; Fuerst, T. R.; Moss, B. *Proc. Natl. Acad. Sci. U.S.A.* **1988**, *85*, 2357.
13. Borkow, G.; Lapidot, A. *Curr. Drug Targets-Infect. Disord.* **2005**, *5*, 3.
14. Harrison, S. C. *Adv. Virus Res.* **2005**, *64*, 231.
15. Cerutti, N.; Mendelow, B. V.; Napier, G. B.; Papathanasopoulos, M. A.; Killick, M.; Khati, M.; Stevens, W.; Capovilla, A. *J. Biol. Chem.* **2010**, *285*, 25743.
16. Kwong, P. D.; Wyatt, R.; Robinson, J.; Sweet, R. W.; Sodroski, J.; Hendrickson, W. A. *Nature* **1998**, *393*, 648.
17. Huang, C.; Tang, M.; Zhang, M. Y.; Majeed, S.; Montabana, E.; Stanfield, R. L.; Dimitrov, D. S.; Korber, B.; Sodroski, J.; Wilson, I. A. *Science* **2005**, *310*, 1025.
18. Diskin, R.; Marcovecchio, P. M.; Bjorkman, P. J. *Nat. Struct. Mol. Biol.* **2010**, *17*, 608.
19. Huang, C.; Lam, S. N.; Acharya, P.; Tang, M.; Xiang, S. H.; Hussan, S. S.; Stanfield, R. L.; Robinson, J.; Sodroski, J.; Wilson, I. A. *Science* **2007**, *317*, 1930.
20. Huang, C.; Venturi, M.; Majeed, S.; Moore, M. J.; Phogat, S.; Zhang, M. Y.; Dimitrov, D. S.; Hendrickson, W. A.; Robinson, J.; Sodroski, J. *Proc. Natl. Acad. Sci. U.S.A.* **2004**, *101*, 2706.
21. Zhou, T.; Xu, L.; Dey, B.; Hessell, A. J.; Van Ryk, D.; Xiang, S. H.; Yang, X.; Zhang, M. Y.; Zwick, M. B.; Arthos, J. *Nature* **2007**, *445*, 732.
22. LaLonde, J. M.; Kwon, Y. D.; Jones, D. M.; Sun, A. W.; Courter, J. R.; Soeta, T.; Kobayashi, T.; Princiotto, A. M.; Wu, X.; Schon, A. *J. Med. Chem.* **2012**, *55*, 4382.
23. Wyatt, R.; Kwong, P. D.; Desjardins, E.; Sweet, R. W.; Robinson, J.; Hendrickson, W. A.; Sodroski, J. G. *Nature* **1998**, *393*, 705.
24. Wang, T.; Zhang, Z.; Wallace, O. B.; Deshpande, M.; Fang, H.; Yang, Z.; Zadjura, L. M.; Tweedie, D. L.; Huang, S.; Zhao, F. *J. Med. Chem.* **2003**, *46*, 4236.
25. Yang, Z.; Zadjura, L.; D'Arienzo, C.; Marino, A.; Santone, K.; Klunk, L.; Greene, D.; Lin, P. F.; Colonno, R.; Wang, T. *Biopharm. Drug Dispos.* **2005**, *26*, 387.
26. Madani, N.; Perdigoto, A. L.; Srinivasan, K.; Cox, J. M.; Chruma, J. J.; LaLonde, J.; Head, M.; Smith Iii, A. B.; Sodroski, J. G. *J. Virol.* **2004**, *78*, 3742.
27. Lin, P. F.; Blair, W.; Wang, T.; Spicer, T.; Guo, Q.; Zhou, N.; Gong, Y. F.; Wang, H. G. H.; Rose, R.; Yamanaka, G. *Proc. Natl. Acad. Sci. U.S.A.* **2003**, *100*, 11013.
28. Teixeira, C.; Serradji, N.; Maurel, F.; Barbault, F. *Eur. J. Med. Chem.* **2009**, *44*, 3524.
29. Gadhe, C. G.; Kothandan, G.; Madhavan, T.; Cho, S. J. *Med. Chem. Res.* **2012**, *21*, 1892.
30. Kong, R.; Tan, J. J.; Ma, X. H.; Chen, W. Z.; Wang, C. X. *BBA-Proteins & Proteomics* **2006**, *1764*, 766.
31. Yang, Q.; Stephen, A. G.; Adelsberger, J. W.; Roberts, P. E.; Zhu, W.; Currens, M. J.; Feng, Y.; Crise, B. J.; Gorelick, R. J.; Rein, A. R. *J. Virol.* **2005**, *79*, 6122.
32. Gadhe, C. G.; Madhavan, T.; Kothandan, G.; Lee, T. B.; Lee, K.; Cho, S. J. *Bull. Korean Chem. Soc.* **2011**, *32*, 1605.
33. Gadhe, C. G.; Kothandan, G.; Cho, S. J. *Mol. Simulat.* **2012**, *38*, 861.
34. Gadhe, C. G.; Lee, S. H.; Madhavan, T.; Kothandan, G.; Choi, D. B.; Cho, S. J. *Bull. Korean Chem. Soc.* **2010**, *31*, 2761.
35. Kothandan, G.; Gadhe, C. G.; Madhavan, T.; Cho, S. J. *Chem. Biol. Drug Des.* **2011**, *78*, 161.
36. Kothandan, G.; Gadhe, C. G.; Cho, S. J. *PLoS One* **2012**, *7*, e32864.
37. Gadhe, C. G.; Kothandan, G.; Cho, S. J. *J. Biomol. Struct. Dyn.* 2012, DOI: 10.1080/07391102.2012.732342.
38. Gadhe, C. G.; Madhavan, T.; Kothandan, G.; Cho, S. J. *BMC Struct. Biol.* **2011**, *11*, 5.
39. Kothandan, G.; Gadhe, C. G.; Madhavan, T.; Choi, C. H.; Cho, S. J. *Eur. J. Med. Chem.* **2011**, *46*, 4078.
40. Madhavan, T.; Chung, J. Y.; Kothandan, G.; Gadhe, C. G.; Cho, S. J. *Chem. Biol. Drug Des.* **2012**, *79*, 53.
41. Lu, R. J.; Tucker, J. A.; Pickens, J.; Ma, Y. A.; Zinevitch, T.; Kirichenko, O.; Konoplev, V.; Kuznetsova, S.; Sviridov, S.; Brahmachary, E. *J. Med. Chem.* **2009**, *52*, 4481.
42. SYBYL U.S.A., 2008.
43. Word, J. M.; Lovell, S. C.; Richardson, J. S.; Richardson, D. C. *J. Mol. Biol.* **1999**, *285*, 1735.
44. Morris, G. M.; Goodsell, D. S.; Halliday, R. S.; Huey, R.; Hart, W. E.; Belew, R. K.; Olson, A. J. *J. Comput. Chem.* **1998**, *19*, 1639.
45. Cordonnier, A.; Montagnier, L.; Emerman, M. *Nature* **1989**, *340*, 571.
46. Olshevsky, U.; Helseth, E.; Furman, C.; Li, J.; Haseltine, W.; Sodroski, J. *J. Virol.* **1990**, *64*, 5701.
47. Hess, B.; Kutzner, C.; Van Der Spoel, D.; Lindahl, E. *J. Chem. Theory Comput.* **2008**, *4*, 435.
48. Oostenbrink, C.; Villa, A.; Mark, A. E.; Van Gunsteren, W. F. *J. Comput. Chem.* **2004**, *25*, 1656.
49. Aalten, D. M. F.; Bywater, R.; Findlay, J. B. C.; Hendlich, M.; Hooft, R. W. W.; Vriend, G. *J. Comput.-Aided Mol. Des.* **1996**, *10*, 255.
50. Hermans, J.; Berendsen, H. J. C.; Van Gunsteren, W. F.; Postma, J. P. M. *Biopolymers* **1984**, *23*, 1513.
51. Darden, T.; York, D.; Pedersen, L. *J. Chem. Phys.* **1993**, *98*, 10089.
52. Miyamoto, S.; Kollman, P. A. *J. Comput. Chem.* **1992**, *13*, 952.
53. Hess, B. *J. Chem. Theory Comput.* **2008**, *4*, 116.
54. Berendsen, H. J. C.; Postma, J. P. M.; Van Gunsteren, W. F.; DiNola, A.; Haak, J. R. *J. Chem. Phys.* **1984**, *81*, 3684.
55. Shrivastava, I.; LaLonde, J. M. *Biochemistry* **2011**, *50*, 4173.
56. Moebius, U.; Clayton, L. K.; Abraham, S.; Harrison, S. C.; Reinherz, E. L. *J. Exp. Med.* **1992**, *176*, 507.
57. Sweet, R. W.; Truneh, A.; Hendrickson, W. A. *Curr. Opin. Biotech.* **1991**, *2*, 622.
58. Stricher, F.; Martin, L.; Barthe, P.; Pogenberg, V.; Mechulam, A.; Menez, A.; Roumestand, C.; Veas, F.; Royer, C.; Vita, C.; *Biochem. J.* **2005**, *390*, 29.